Multi-Modulation Scheme for RFID-based Sensor Networks

Zijing Tian[1] and Zygmunt J. Haas[1,2]
[1] School of Engineering and Computer Science, University of Texas at Dallas, Richardson, TX
[2] School of Electrical and Computer Engineering, Cornell University, Ithaca, NY
zxt140530@utdallas.edu, zhaas@cornell.edu

Abstract. RFID technology is playing an increasingly more important role in the *Internet of Things*, especially in the dense deployment model. In such networks, in addition to communication, nodes may also need to harvest energy from the environment to operate. In particular, we assume that our network model relies on RFID sensor network consisting of Wireless Identification and Sensing Platform (WISP) devices and RFID exciters. In WISP, the sensors harvest ambient energy from the RFID exciters and use this energy for communication back to the exciter. However, as the number of exciters is typically small, sensors further away from an exciter will need longer charging time to be able to transmit the same amount of information than a closer by sensor. Thus, further away sensors limit the overall throughput of the network. In this paper, we propose to use a multi-modulation scheme, which trades off power for transmission duration. More specifically, in this scheme, sensors closer to the exciter use a higher-order modulation, which requires more power than a lower-order modulation assigned to further away sensors, for the same bit error rate of all the sensors' transmissions. This reduces the transmission time of the closer sensors, while also reducing the charging time of the further away sensors, overall increasing the total network throughput. The evaluation results show that the RFID sensor network with our multi-modulation scheme has significantly higher throughput as compared with the traditional single-modulation scheme.

Keywords: RFID systems; IoT; WISP; energy harvesting; multi-modulation scheme; throughput optimization; sensor network

1 Introduction and Motivation

The *Internet of Things* (IoT) networking paradigm continues to draw a lot of attention, especially with the deployment of novel and exciting applications, many of which requiring dense deployment of sensing/processing/communicating devices ("things"). At the same time, radio frequency identification (RFID) technologies and RFID sensor networks (RSNs), which consist of exciters and RFID nodes, promise to broaden RFID systems by incorporating sensing technologies [1]. Nodes in RSNs are Wireless Identification and Sensing Platform (WISP)[1] sensor devices which are capable of harvesting

[1] RSNs and especially the WISP technology is extensively discussed in [1-4].

their operating energy from RFID transmissions [2]. The problem that we investigate in this paper relates to energy harvesting by sensor nodes in RSN with dense deployment.[2]

In general, an RSN consists of sensor nodes and RFID *exciters*[3] deployed among the nodes. The RFID exciters transmit to the RFID devices by continuous wave (CW) signals, and the sensor nodes convert these signals to DC, charging their on-board energy storage elements (e.g., a super capacitor). When a sensor node accumulates enough energy from an exciter, it will be able to transmit their own signals back to the exciter. In this study, we adopt a combination of RFID tags and sensors [3] functioning as sensor nodes capable of energy harvesting. This kind of sensor nodes could gather information by its sensor, harvest and store energy in the sensor node, and then send the information to the exciter upon receiving permission from the exciter. (The energy harvesting circuit is similar to the circuit in semi-passive tag-based sensor nodes [4]. And although our system model does not employ passive backscattering techniques, other systems models could be considered in future work.

RFID technology is already pervasive in applications such as bar codes [5] and applying the technology to IoT system is becoming widespread in Smart Cities and in Smart Homes projects [6]. RFID technology has also been extensively deployed in various and distinctive fields, such as access control, biomedical implants, identification, tracking, logistics, sensor networks, security, fast payment system, loss prevention and shopping malls [7]. The use of WISP devices as RFID sensor nodes augments the RFID technology with increased computational capabilities [1].

With the growing demand for large size RSNs, the energy harvesting efficiency becomes a constraint that limits the throughput of a sensor network. This paper is aiming at the optimization of RSN communication in dense sensor nodes deployment [8]. In this kind of RSNs, nodes which are deployed further from the exciter experience larger attenuation of the CW signal, and thus will be charged at a slower pace than nodes located closer to the reader. Furthermore, such further-away nodes require more energy to transmit back to the exciter (again because of the signal attenuation with distance) to achieve the same bit error rate (BER) as nodes located close-by to the exciter. Thus, the required charging time is prolonged by the "ineffective energy harvesting" of the far-away nodes, reducing the overall throughput of the whole RSN.

To address this limitation, we propose a multi-modulation scheme, where based on a node's distance from the exciter, different modulation methods are used by the network's nodes. Although RFID system that apply different modulation schemes were previously proposed in [9], however, that work didn't provide any strategy to improve the performance of the RFID system by the use of multi-modulation. In our study, we focus on the RSN design of such multi-modulation-based RFID sensor networks to significantly improve the network's performance. Since different modulation methods have different Signal to Noise Ratio (SNR) requirements, we can balance the energy harvesting effectiveness of the different nodes by applying the different modulation

---

[2] Imagine that the hardware of a dense IoT device requires changing a battery once in 4 years. In a deployment of 100,000 devices, this means that there is a need to replace 2,500 batteries every year or ~70 batteries every day!

[3] The terms "reader" and "exciter" are interchangeably used in technical literature.

schemes according to the sensor nodes' distances to the exciter. In our work, we assume that there is a single channel that is used sequentially by the sensor nodes to transmit. Since one transmission cycle for the RSN consists of the charging time in addition to the transmission times of all the nodes, to maximize the network throughput, we need to reduce the sum of these two components. Because higher order modulation methods result in shorter transmission times (as discussed in Section 3), the multi-modulation scheme needs to judiciously trade-off between the transmission time and the required charging time, as to minimize the overall performance. In other words, the multi-modulation scheme allows: (1) saving the overall charging time compared with the case of a single modulation scheme, and (2) saving the overall transmission time compared with the case of a single modulation scheme. In summary, the result shows that our multi-modulation scheme has a significant improvement in throughput of the RSN, as compared with the traditional single-modulation scheme.

The rest of the paper is organized as follows: In Section 2, we introduce our multi-modulation scheme, with the theoretical results of the scheme presented in Section 3. In Section 4, we show how our scheme works in a multi-exciter environment. In Section 5, we present numerical results that demonstrate the improvement of our scheme compared with the traditional single-modulation scheme. Section 6 concludes the paper.

2 Multi Modulation Scheme

In the proposed multi-modulation scheme for RFID sensor networks hundreds/thousands of sensor nodes are deployed in the RFID reader coverage area. We assume that nodes in the coverage area follow a uniform distribution, and that the communication requirements (i.e., the amounts of data) that all the nodes need to transmit to the exciter are the same. An RFID exciter (sometimes referred to as a *reader*) emits CW signals to supply energy to sensor nodes in the coverage area. The exciter also serves as a router that is responsible for scheduling data transmissions of the sensor nodes and for receiving messages from nodes. Sensor nodes are designed to harvest energy from the ambient RF signal of the exciter, using known energy harvesting techniques in the RFID systems, as are known to be applied to semi-passive tags [10]. A sensor node can transmit its message only after it has been sufficiently charged and it receives the permission from the exciter. In our model, we assume that sensor nodes cannot harvest energy and transmit data to the exciter at the same time (i.e., all the harvested energy is used to charge the sensor node's energy storage).

In our RSN, all the sensor nodes within the exciter coverage area share one communication channel. As the exciter arranges the schedule of the sensor nodes' transmissions in each cycle, the exciter needs to query each node within its coverage area in each transmission cycle whether the node has data to transmit. The amount of data that each node transmits in a cycle is the same for all the nodes and the symbol rate (discussed in Section 3) for all the node-to-exciter transmissions is the same for all the nodes. Thus, the bandwidth requirements of all the nodes are the same too. Since we want to improve the throughput of the RFID sensor network and the throughput of a network has an inverse relation to the cycle time, the cycle time needs to be minimized.

As shown in Fig. 1, there are three major phases in a transmission cycle: Query, Charging, and Transmissions. In the Query phase, the exciter identifies the sensor nodes that have data to transmit. (We note that if the network allows the set of sensor nodes to change over time, this phase could also be used to discover nodes in the coverage area.) Since before any node can transmit it needs to collect sufficient energy, the Query phase includes a short charging time (not shown in the figure) to allow a node to respond to the exciter's query. Based on the nodes' responses, the exciter starts sending CW (in the Charging phase) to sufficiently charge the nodes. The exciter then sequentially sends short polling messages to the next node that is scheduled to transmit (not shown in the figure), so that the nodes can transmit their data. Only nodes who announced to the exciter in the Query phase that they have data to transmit will be polled in this Transmissions phase.

Fig. 1: Phases of a transmission cycle

In general, the charging time period depends on the required charging time of the furthest node, which is determined by the exciter-to-node distance R. To maximize the network throughput, we apply a family of modulation schemes (e.g., PSK) to the nodes in the network, where the further away nodes are assigned such an order of the modulation family (e.g., 8-PSK or 16-PSK) that requires less power to transmit. This way, in each cycle of data transmission, our network will take a shorter time to finish all the transmissions than when a single-modulation scheme is used by all the nodes. In general, the total transmission time of a cycle in this scheme is:

$$t_{total} = t_{query} + \sum t_{transmit} + \mathrm{Max}(t_{charge}) \,, \tag{1}$$

where t_{query} is the time needed for the Query phase, $\sum t_{transmit}$ is the summation of the transmission times of all the sensor nodes, and $\mathrm{Max}(t_{charge})$ represents the maximum charging time among all the nodes. Thus, the charging time needed for the whole network depends on the charging time of the sensor node that needs the most time to charge, while the transmission time for the whole network depends on the summation of the all the transmission times of the nodes, because we assume a single channel, so that the exciter cannot receive signals from different nodes at the same time.

Since different modulation schemes require different levels of the energy-per-bit to noise-power-spectral-density ratio ($\frac{E_b}{N_0}$) to achieve the same bit error rate (BER), the energy-per-bit, E_b, required for different modulations are also different. If we apply the same modulation scheme to all the sensor nodes, the closer nodes would need to wait for the further nodes to finish charging. However, if we assign to the furthest nodes a modulation scheme that requires less energy to transmit, the charging time for the nodes will decrease; thus, the total cycle time will decrease as well. The motivation behind our scheme is as follows. Since in this network, the symbol rate of the system remains the

same for all the nodes, modulation schemes that require less energy to transmit results in a less charging time but longer transmission time (as discussed in Section 3). Consequently, assume we have modulation schemes A and B, and nodes applying the scheme A require less energy to transmit per bit than nodes applying the scheme B, while the latter can transmit more bits per unit time. Thus, we can apply scheme A to the further nodes, and apply scheme B to the closer nodes. Since applying modulation scheme B will reduce the transmission time of the closer nodes, the total transmission time will be reduced compared with networks that only apply the modulation scheme A; and because the modulation scheme A reduces the charging time of the whole network, the multi-modulation scheme has a shorter cycle time compared with networks that only apply the modulation scheme B. Hence, the sum of transmission time and charging time (i.e., eq. (1)) could be optimized under our multi-modulation scheme. To summarize, the scheme that we propose in this paper applies different modulation methods to sensor nodes according to their distance to exciter R, as to optimize the throughput of the network.

We first calculate the maximum RFID exciter-to-node range R. There are two main criteria to constrain the maximum range of exciter-to-node communication (further discussed in Section 3): (1) the reading range of the RFID exciter, and (2) the required BER of the application. The first criterion determines the furthest possible range of exciter coverage area (R_{cover}), and the second criterion determines the furthest range of exciter-to-node communication for particular modulations (R_{max}) under particular charging time limitation. Although we can extend the charging time to increase R_{max}, R_{max} cannot be larger than R_{cover}.

The references [11] – [18] outline the main modulation schemes used for RFID UHF schemes: QAM, QPSK, BPSK, ASK, and OOK.[4]. We choose PSK, PAM, and QAM [12] modulations with different number of bits per symbol k ($\mathrm{M} = 2^k$), because they are the more commonly used schemes in RFID systems.

In the particular example presented in Section 5, we apply three different orders of the PSK family of modulations: QPSK, 8-PSK, and 16-PSK to the 100 sensor nodes in the exciter coverage area. These 100 nodes are deployed within the area determined by the QPSK modulation scheme, $R_{\max(QPSK)}$. The exciter's coverage area is divided into four areas: (1) the circle with 16-PSK modulation, where the distance of the nodes to the exciter is no larger than $R_{\max(16-PSK)}$; (2) the annulus region with 8-PSK modulation, where the distance of the nodes to the exciter is between $R_{\max(16-PSK)}$ and $R_{\max(8-PSK)}$; (3) the annulus region with QPSK modulation, where the distance of nodes to the exciter is between $R_{\max(8-PSK)}$ and $R_{\max(QPSK)}$. Fig. 2 shows the region partition for our multi-modulation scheme.

[4] We do not use the OOK modulation scheme, since with this modulation we cannot apply different number of bits per symbol, k [17].

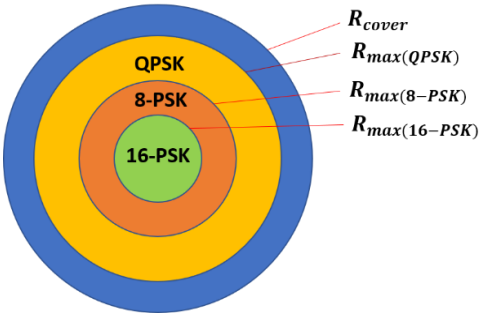

Fig. 2: The region partition and assignments of the modulation schemes

Although we divided the coverage area into the three regions above, the distances of the sensor nodes to the exciter within each ring are not exactly the same. Thus, the length of the charging phase is determined by the node with the largest required charging time; i.e., a node that is the furthest distance from the exciter and is still in its ring area; in other words, a node located on the boundary to the next ring.

3 Derivation of the Multi-modulation Scheme Improvement

In this section, we derive the performance improvement of our multi-modulation scheme. First, we briefly discuss the basic concepts used throughout this section. In this study, the BER required by the application is the main design criterion that limits the node-to-exciter communication range. For a particular modulation scheme, the $\frac{E_b}{N_0}$ has a direct relation to BER. SER represents the symbol error rate, with the energy per symbol $E_s = k \times E_b$ being another parameter in our research, where k represents the number of bits-per-symbol of a particular modulation scheme [19]. We also consider an additive white Gaussian noise (AWGN) in our work [19].

According to the requirement of the modulation methods assignment in Fig. 2, we should first figure out the $\frac{E_b}{N_0}$ of the different modulation schemes based on the same required BER, so that we can determine the partition rings of our scheme. The SER-SNR and BER-SNR formulas of the various modulation schemes are shown in Table 1 [20].

Table 1. SER v. SNR and BER v. SNR for various modulation orders

	K=1	K=2	K=3
SER	$Q(\sqrt{2\frac{E_s}{N_0}})$	$2Q(\sqrt{2\frac{E_s}{N_0}})$	$2Q(\sqrt{2\frac{E_s}{N_0}}sin\frac{\pi}{M})$
BER	$Q(\sqrt{2\frac{E_b}{N_0}})$	$Q(\sqrt{2\frac{E_b}{N_0}})$	$\frac{2}{k}Q(\sqrt{2k\frac{E_b}{N_0}}sin\frac{\pi}{M})$

Using the Table 1 and the inverse Q-function, one can derive the required $\frac{E_b}{N_0}$ for a particular value of BER. Then for a choice of M-PSK, we obtain the formulas for $\frac{E_b}{N_0}$ and $\frac{E_S}{N_0}$ in Table 2 [20].

Table 2. $\frac{E_S}{N_0}$ and $\frac{E_b}{N_0}$ as a function of SER for various M-PSK modulations

	BPSK	QPSK	M-PSK(M>4)
$\frac{E_s}{N_0}$	$(erfc^{-1}(SER))^2$	$2(erfc^{-1}(SER))^2$	$\frac{2(erfc^{-1}(SER))^2}{2(sin\frac{\pi}{M})^2}$
$\frac{E_b}{N_0}$	$(erfc^{-1}(BER))^2$	$(erfc^{-1}(BER))^2$	$\frac{(erfc^{-1}(\frac{k}{2}BER))^2}{k(sin\frac{\pi}{M})^2}$

Next, we study the energy transfer in our RFID sensor network to find the exact criterion for R_{max}. The downlink power which shows the exciter-to-node power received at the sensor nodes, P_{node}, is:

$$P_{node} = P_{cw}(\frac{\lambda_{cw}}{4\pi R})^2 G_{exciter} G_{node}, \quad (2)$$

where P_{cw} is the power of the CW emitted from the exciter, R is the distance between the exciter and a sensor node, λ_{cw} is the wavelength of the CW signal, $G_{exciter}$ and G_{node} are the power gains of the exciter and node antennas, respectively [21], and all powers are expressed in units of Watts.

For the uplink power, the node-to-exciter power received at the exciter, P_{rd}, is:

$$P_{rd} = P_{back}(\frac{\lambda_{cw}}{4\pi R})^2 G_{exciter} G_{node}, \quad (3)$$

where P_{back} is the modulated power emitted by a sensor node. By studying the relationship between P_{back} and P_{node}, we can find the modulation region partition in Fig. 2. If we label the power efficiency of energy harvesting in the nodes as ρ_t, the charging time in each cycle as t_{charge}, and the time duration that a node transmits in each cycle as $t_{transmit}$, the relationship between P_{back} and P_{node} is:

$$P_{back} \cdot t_{transmit} = \rho_t \cdot P_{node} \cdot t_{charge}, \quad (4)$$

where $t_{transmit} = L/R_b$ is the transmission time needed for transmission of L bits (i.e., L is the length of the data needed to be transmitted (in bits)), and R_b is the bit rate. We assume the symbol rate S_b (in units of symbols/sec) is fixed for all the network transmissions. Thus, the data rates R_b of the different modulations with different bits-per-symbol are different, because $R_b = k \times S_b$. The bandwidth B of the PSK/QAM modulated signal is $B = \frac{2R_b}{k}$ [22]. Hence, $B = 2S_b$, and the same bandwidth is used by all the sensor nodes.

In this study, we use the criteria in reference [23] as the value of R_{cover}, which is 30.5 meter for semi-passive tags, as we assume that our nodes rely on similar circuitry as

semi-passive tags. Next, we concentrate on obtaining R_{max},which is constrained by the acceptable maximum BER for all the modulations. Eq. (5) represents the relationship between P_{rd} and $\frac{E_s}{N_0}$ [24]:

$$\frac{P_{rd}}{N_0} = R_b\left(\frac{E_b}{N_0}\right) = k \times S_b\left(\frac{E_s}{kN_0}\right) = S_b\left(\frac{E_s}{N_0}\right). \tag{5}$$

In our scheme, a sensor node is charged by the exciter as per eq. (2). After a charging time t_{charge}, the node will have enough power to transmit its data of L bits. Then by eq. (4), the power sent back from the node is calculated. The back power received in the exciter, P_{rd}, is calculated by eq. (3). For all the nodes, independent of the modulation scheme, the maximum acceptable BER of the nodes' signals received by the exciter should be the same and is given by the application. Therefore, knowing the required BER, we can find the corresponding required minimum $\frac{E_b}{N_0}$ for PSK modulation with different M by using formulas in Table 1 and Table 2. Then by eq. (5), we obtain the minimum power P_{rd} needed in the exciter for the different modulations:

$$P_{rd(min)} = N_0 S_b\left(\frac{E_s}{N_0}\right) = N_0 S_b k\left(\frac{E_b}{N_0}\right), \tag{6}$$

where $\frac{E_b}{N_0}$ is calculated by formulas in Table 2. Combining eq. (2), (3), (4), and (6), we obtain the constraint of the distance R_{max} for the different modulation schemes:

$$\begin{aligned} N_0 S_b k\left(\frac{E_b}{N_0}\right) &= P_{back}\left(\frac{\lambda_{cw}}{4\pi R_{max}}\right)^2 G_{exciter} G_{node} \\ &= \frac{\rho_t \cdot P_{node} \cdot t_{charge}}{t_{transmit}}\left(\frac{\lambda_{cw}}{4\pi R_{max}}\right)^2 G_{exciter} G_{node} \\ &= \frac{P_{cw} G_{exciter} G_{node} \rho_t t_{charge}}{t_{transmit}}\left(\frac{\lambda_{cw}}{4\pi R_{max}}\right)^4 G_{exciter} G_{node} \end{aligned}$$

$$R_{max} = \sqrt[4]{\frac{P_{cw}\rho_t t_{charge}}{N_0 S_{bk}\left(\frac{E_b}{N_0}\right) t_{transmit}}\left(\frac{\lambda_{cw}}{4\pi}\right)^4 (G_{exciter} G_{node})^2} = \sqrt[4]{\frac{P_{cw}\rho_t t_{charge}}{N_0\left(\frac{E_b}{N_0}\right)_L}\left(\frac{\lambda_{cw}}{4\pi}\right)^4 (G_{exciter} G_{node})^2} \tag{7}$$

Thus R_{max} is determined by the charging time, t_{charge} and by $\frac{E_b}{N_0}$. Since we want the maximum charging time for all the different modulations to be the same, and we assume that all the sensor nodes have the same amount of data L to transmit and the same transmitted symbol rate S_b, we have the relationship between the distances R_1 and R_2 as a function of $\frac{E_{b1}}{N_0}$ and $\frac{E_{b2}}{N_0}$ for two different modulations as:

$$\frac{R_1}{R_2} == \sqrt[4]{\frac{E_{b2}}{N_0} / \frac{E_{b1}}{N_0}}. \tag{8}$$

Then the charging time is calculated as:

$$t_{charge} = \frac{N_0\left(\frac{E_b}{N_0}\right)L}{P_{cw}\rho_t(G_{exciter}G_{node})^2}\left(\frac{4\pi R}{\lambda_{cw}}\right)^4 . \quad (9)$$

Assume that we have n nodes distributed throughout the three regions (in Fig. 2) as follows: x nodes using QPSK, y nodes using 8-PSK, and z nodes using 16-PSK, where $n = x + y + z$, and the furthest node is at the distance of R_{max}. Assuming uniform geographic distribution of the nodes in the network, the number of nodes deployed in the different regions is:

$$x = n \times \frac{A_{(QPSK)}}{A_{(QPSK)} + A_{(8-PSK)} + A_{(16-PSK)}} = \frac{R^2_{\max\,(QPSK)} - R^2_{\max\,(8-PSK)}}{R^2_{\max\,(QPSK)}},$$

$$y = n \times \frac{A_{(8-PSK)}}{A_{(QPSK)} + A_{(8-PSK)} + A_{(16-PSK)}} \frac{R^2_{\max\,(8-PSK)} - R^2_{\max\,(16-PSK)}}{R^2_{\max\,(QPSK)}},$$

$$z = n \times \frac{A_{(16-PSK)}}{A_{(QPSK)} + A_{(8-PSK)} + A_{(16-PSK)}} = \frac{R^2_{\max\,(16-PSK)}}{R^2_{\max\,(QPSK)}}. \quad (10)$$

Based on eq. (10), we can calculate the duration of the cycles in the multi-modulation and in the single-modulation schemes:

$$t_{total-mm} = t_{query} + \sum t_{transmit} + t_{charge(max)} = t_{query} + \frac{L}{k_1 \times S_b}x + \frac{L}{k_2 \times S_b}y + \frac{L}{k_3 \times S_b}z + t_{charge(Max(QPSK))}$$

$$t_{total-sm} = t_{query} + \sum t_{transmit} + t_{charge(max)} = t_{query} + \frac{nL}{k_i \times S_b} + t_{charge(Max(i-PSK))}, \quad (11)$$

where k_i represents the number of bits-per-symbol in the various modulation schemes (i.e., QPSK, 8-PSK, and 16-PSK), and $t_{charge(Max(QSK))} < t_{charge(Max(8-PSK))} < t_{charge(Max(16-PSK))}$ are calculated by eq. (9).

Thus, the reduction of the cycle duration time by our scheme compared with single-modulation scheme is:

$$t_{total-sm} - t_{total-mm} = \frac{nL}{k_i \times S_b} - \frac{L}{k_1 \times S_b}x - \frac{L}{k_2 \times S_b}y - \frac{L}{k_3 \times S_b}z + t_{charge(Max(i-PSK))} - t_{charge(Max(QPSK))} . \quad (12)$$

We note that when we calculate the improvement of the network throughput, our multi-modulation scheme should be compared with the single-modulation scheme that performs the best among all the three single-modulation schemes which are used in our multi-modulation scheme. Hence, the throughput improvement, B_{multi}, is calculated by eq. (13):

$$B_{multi} = \frac{\left(\frac{1}{t_{total(Multi)}} - \frac{1}{MIN\left(t_{total(QPSK)}, t_{total(8-PSK)}, t_{total(16-PSK)}\right)}\right)}{\frac{1}{MIN\left(t_{total(QPSK)}, t_{total(8-PSK)}, t_{total(16-PSK)}\right)}} \quad (13)$$

4 Multi-Modulation Scheme with Multiple Exciters

It is likely that in a large deployment of an RSN, there will be more than one exciter present (e.g., multi-exciter network as in [25]). In this section, we assume that the exciters are uniformly deployed in the network (this is a reasonable assumption, given the fact that the sensor nodes are randomly, but uniformly, distributed too). We also assume that the antennas of the sensor nodes are unidirectional, so that the nodes are able to receive power from different directions at the same time. We consider the locations of the exciters at the centers of a hexagonal grid. Then the received power by a node depends on the distances between the node and the exciters (and is calculated by eq. (2)), and the total received energy of a node is calculated by the sum of their received energy from the all the exciters. Because of the exponential dependence on distance in eq. (2), in calculating the power collected by a sensor node, we need to consider only the closest several exciters to the node, and we can ignore the power received from the other further away exciters.

Consider an area covered by 7 exciters arranged in a hexagonal grid, as depicted in Fig. 3.

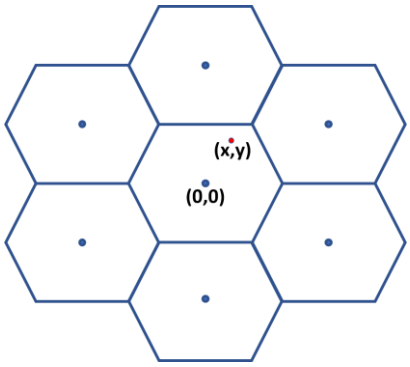

Fig. 3: Structure of a multi-exciter network

Assume that the middle exciter is at the origin, $(0, 0)$, while the coordinates of the other six exciters are: $(0, \sqrt{3}R)$, $(\frac{3}{2}R, \frac{\sqrt{3}}{2}R)$, $(\frac{3}{2}, -\frac{\sqrt{3}}{2}R)$, $(0, -\sqrt{3R})$, $(-\frac{3}{2}R, \frac{\sqrt{3}}{2}R)$, and $(-\frac{3}{2}R, -\frac{\sqrt{3}}{2}R)$. We label the coordinates of an exemplary node in the middle of the hexagonal grid as (x, y). The power received by the exemplary node in the central hexagon is:

$$P_{node}(x,y) = P_{cw}(\frac{\lambda_{cw}}{4\pi})^2 G_{exciter} G_{node} \times \left(\frac{1}{x^2+y^2} + \frac{1}{x^2+\left(y-\sqrt{3R}\right)^2} + \frac{1}{x^2+\left(y+\sqrt{3R}\right)^2} + \right.$$

$$\left. \frac{1}{\left(x-\frac{3}{2}R\right)^2+\left(y-\frac{\sqrt{3}}{2}R\right)^2} + \frac{1}{\left(x-\frac{3}{2}R\right)^2+\left(y+\frac{\sqrt{3}}{2}R\right)^2} + \frac{1}{\left(x+\frac{3}{2}R\right)^2+\left(y-\frac{\sqrt{3}}{2}R\right)^2} + \frac{1}{\left(x+\frac{3}{2}R\right)^2+\left(y+\frac{\sqrt{3}}{2}R\right)^2} \right) \quad (14)$$

The level of the received power (displayed only for the central hexagon) as a function of the node's location, $(x,\ y)$, is shown in Fig. 4.

Next, we study the behavior of eq. (14) for different locations of the sensor node, $(x,\ y)$. More specifically, we show that $P_{node}(x,y)$ is a strictly increasing function as we move the location of the node from a boundary of the hexagon to its vertex.

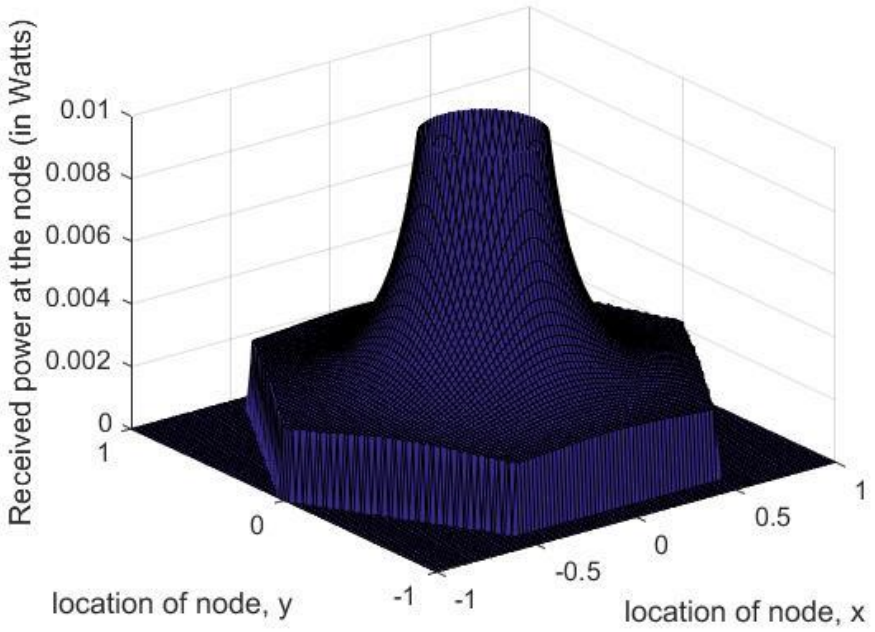

Fig. 4: The received power plot as a function of the sensor node's location in the central hexagon (the plot is truncated at received power of 0.01W)

Using the polar coordinate system, where $x = r\cos\theta\,, y = r\cdot\sin\theta;\ r$ is the distance from node to the origin, and θ is the angle of node location relative to the $x-$axis, eq. (14) can be rewritten as:

$$P_{node}(r,\theta) = P_{cw}\left(\frac{\lambda_{cw}}{4\pi}\right)^2 G_{exciter}G_{node} \times \left(\frac{1}{r^2} + \frac{1}{r^2+3R^2-2\sqrt{3}rR\sin\theta} + \frac{1}{r^2+3R^2+2\sqrt{3}rR\sin\theta} + \frac{1}{r^2+3R^2-3rR\cos\theta-\sqrt{3}rR\sin\theta} + \frac{1}{r^2+3R^2-3rR\cos\theta+\sqrt{3}rR\sin\theta} + \frac{1}{r^2+3R^2+3rR\cos\theta-\sqrt{3}rR\sin\theta} + \frac{1}{r^2+3R^2+3rR\cos\theta+\sqrt{3}rR\sin\theta}\right) \quad (15)$$

Now, taking a derivative of $P_{node}(r,\theta)$ with respect to r, one can easily verify that $\partial P_{node}(r,\theta)/\partial r < 0$. Hence, the received power gain in any direction is a monotonically increasing function from the boundary to the vertex of a hexagon. Furthermore, as can be demonstrated by eq. (15) (and is also evident in Fig. 5), there exists r_0 for which the received power at a node is relatively constant for $r_0 \le r \le 1$. This indicates that the sensor nodes in the area $r_0 \le r \le 1$ could be assigned the same modulation scheme. Combining eq. (15) with eqs. (3), (4), and (6), we obtain the region partition formula for any direction θ from the center of a hexagon to its edge:

$$\frac{\left(\frac{E_{b1}}{N_0}\right)}{\left(\frac{E_{b2}}{N_0}\right)} = \quad (16)$$

$$\frac{\left(r_2^2\left(\frac{\frac{1}{r_1^2} + \frac{1}{r_1^2+3R^2-2\sqrt{3}r_1R\sin\theta} + \frac{1}{r_1^2+3R^2+2\sqrt{3}r_1R\sin\theta} + \frac{1}{r_1^2+3R^2-3r_1R\cos\theta-\sqrt{3}r_1R\sin\theta} + \frac{1}{r_1^2+3R^2-3r_1R\cos\theta-\sqrt{3}r_1R\sin\theta} + \frac{1}{r_1^2+3R^2+3r_1R\cos\theta+\sqrt{3}r_1R\sin\theta}}{\frac{1}{r_1^2+3R^2-3r_1R\cos\theta+\sqrt{3}r_1R\sin\theta} + \frac{1}{r_1^2+3R^2+3r_1R\cos\theta-\sqrt{3}r_1R\sin\theta} + \frac{1}{r_1^2+3R^2+3r_1R\cos\theta+\sqrt{3}r_1R\sin\theta}}\right)\right)}{\left(r_1^2\left(\frac{\frac{1}{r_2^2} + \frac{1}{r_2^2+3R^2-2\sqrt{3}r_2R\sin\theta} + \frac{1}{r_2^2+3R^2+2\sqrt{3}r_2R\sin\theta} + \frac{1}{r_2^2+3R^2-3rR\cos\theta-\sqrt{3}r_2R\sin\theta} + \frac{1}{r_2^2+3R^2-3r_2R\cos\theta+\sqrt{3}r_2R\sin\theta} + \frac{1}{r_2^2+3R^2+3r_2R\cos\theta+\sqrt{3}r_2R\sin\theta}}{\frac{1}{r_2^2+3R^2-3r_2R\cos\theta+\sqrt{3}r_2R\sin\theta} + \frac{1}{r_2^2+3R^2+3r_2R\cos\theta-\sqrt{3}r_2R\sin\theta} + \frac{1}{r_2^2+3R^2+3r_2R\cos\theta+\sqrt{3}r_2R\sin\theta}}\right)\right)},$$

where r_1 is the furthest exciter-to-node distance for modulation scheme 1, and r_2 is the furthest exciter-to-node distance for modulation scheme 2. For example, using QPSK modulation as modulation scheme 1, $r_1 = r_{\max(QPSK)}$. Let $u_1 = \frac{R}{r_1}$, $u_2 = \frac{R}{r_2}$, eq. (16) is now changed to:

$$\frac{\left(\frac{E_{b1}}{N_0}\right)}{\left(\frac{E_{b2}}{N_0}\right)} = \quad (17)$$

$$\frac{\left(u_1^4\left(\frac{1 + \frac{1}{1+3u_1^2-2\sqrt{3}u_1\sin\theta} + \frac{1}{1+3u_1^2+2\sqrt{3}u_1\sin\theta} + \frac{1}{1+3u_1^2-3u_1\cos\theta-\sqrt{3}u_1\sin\theta} + \frac{1}{1+3u_1^2-3u_1\cos\theta+\sqrt{3}u_1\sin\theta} + \frac{1}{1+3u_1^2+3u_1\cos\theta-\sqrt{3}u_1\sin\theta} + \frac{1}{1+3u_1^2+3u_1\cos\theta+\sqrt{3}u_1\sin\theta}}\right)\right)}{\left(u_2^4\left(\frac{1 + \frac{1}{1+3u_2^2-2\sqrt{3}u_2\sin\theta} + \frac{1}{1+3u_2^2+2\sqrt{3}u_2\sin\theta} + \frac{1}{1+3u_2^2-3u_2\cos\theta-\sqrt{3}u_2\sin\theta} + \frac{1}{1+3u_2^2-3u_2\cos\theta+\sqrt{3}u_2\sin\theta} + \frac{1}{1+3u_2^2+3u_2\cos\theta-\sqrt{3}u_2\sin\theta} + \frac{1}{1+3u_2^2+3u_2\cos\theta+\sqrt{3}u_2\sin\theta}}\right)\right)},$$

As represented in eq. (17), since we use the ratio of r_1 to R, or r_2 to R instead of an actual value of R, the region partition principle is not dependent on the value of R. Thus, in our example of a multi-exciter network, the region partition for the three modulations

is shown in Fig. 5. For each direction θ, the relation between $r_{\max\,(QPSK)}$, $r_{\max\,(8-PSK)}$, and $r_{\max\,(16-PSK)}$, should follow eq. (16) or eq. (17).

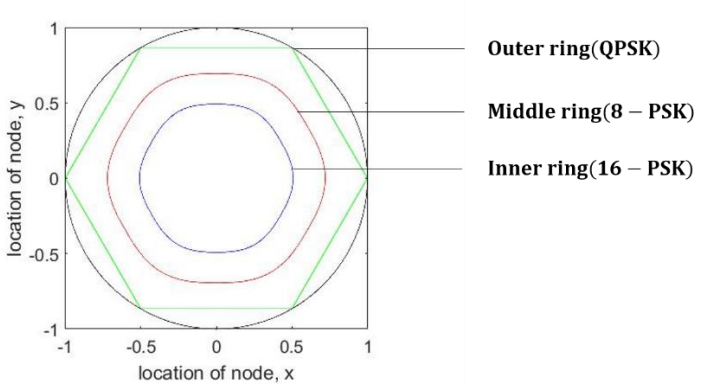

Fig. 5: Partition of the hexagon area by three modulation type (QPSK, 8-PSK, and 16-PSK) in a multi-exciter network

In Fig. 5, there are three rings: the black (outer) ring represents the boundary of QPSK; the red (middle) ring represents the boundary for 8-PSK; and the blue (inner) ring represents the boundary for 16-PSK. The area between hexagon boundary (green lines) and the middle ring is the region where QPSK is used by the nodes in this hexagonal area; the area between the middle ring and the inner ring is the region where 8-PSK is used by the nodes in this hexagon; the area within the inner ring is the region where 16-PSK is used by the nodes in this hexagon. The area between the outer ring and hexagon boundary will apply QPSK as well; however, since this area belongs partially to other hexagon regions, some nodes in this area are assigned to the other exciters based on the region partition by the hexagonal grid.

If we have a sensor node using modulation scheme 1 where $u_1 = \frac{R}{r_1}$, we can calculate the charging time for this node in one cycle by eq. (18) which is extension of eq. (9) and by eq. (17) which presents the charging time of sensor nodes in multi-exciter scheme (proof omitted):

$$t_{charge-me} = \frac{\frac{N_0\left(\frac{E_{b1}}{N_0}\right)L}{P_{cw}\rho_t(G_{exciter}G_{node})^2}\left(\frac{4\pi}{\lambda_{cw}}\right)^4 \cdot r_1^4}{\left(1+\frac{1}{1+3u_1^2-2\sqrt{3}u_1\sin\theta}+\frac{1}{1+3u_1^2+2\sqrt{3}u_1\sin\theta}+\frac{1}{1+3u_1^2-3\,u_1\cos\theta-\sqrt{3}u_1\sin\theta}+\frac{1}{1+3u_1^2-3u_1\cos\theta+\sqrt{3}u_1\sin\theta}+\frac{1}{1+3u_1^2+3\,u_1\cos\theta-\sqrt{3}u_1\sin\theta}+\frac{1}{1+3u_1^2+3\,u_1\cos\theta+\sqrt{3}u_1\sin\theta}\right)} \quad (18)$$

5 Numerical Results

In IEEE 802.15.4 standard [26], the UHF communication frequencies are specified as 868 [MHz], 915 [MHz], and 2.45 [GHz]. Those frequencies could be applied in RFID systems [27]. In our scheme, we also assume a fixed symbol rate of 200kHz as per [11], which allows at most 32-PSK modulation in the IEEE 802.15.4 standard.

Now we will calculate the numerical result of R_{max} in a single exciter network for QPSK, 8-PSK and 16-PSK, using Tables 1-2 and equations in Section 3.

We assume the following parameter values: BER threshold of 10^{-6} [28], $\gamma_{b(QPSK)} = 10.779dB$, $\gamma_{b(8-PSK)} = 14.205dB, \gamma_{b(16-PSK)} = 18.7dB$ (using Table 2), $P_{cw} = 1W$, $G_{exciter} = 6dBi$, $G_{node} = 2dBi$, $\lambda_{cw} = 0.12245m$ (for frequency of $2.45GHz$), and $N_0 = -140dbm/Hz$ [29,30]. We further assume that L=16 kb [31] as the message size to transmit, $S_b = 200kHz$ [11], and ρ_t=0.6667 [24,32]. We use three levels of PSK modulations: QPSK, 8-PSK, and 16-PSK, so that $t_{transmit} = \frac{L}{k \times S_b}, t_{transmit(k=2)} = 0.04sec, t_{transmit(k=3)} = 0.00268sec,$ and $t_{transmit(k=4)} = 0.02sec$. R_{cover}= 30.5m [23].

The charging time is then calculated by eq. (9). If, as an example, $R_{\max(QPSK)} = 20m$, then $t_{charge} = 1.2798s$.

For *k*=3, the 8-PSK boundary, which is the middle ring, by eq.(8):

$$R_{\max(8-PSK)} = 20 \times \sqrt[4]{\frac{10^{1.0778}}{10^{1.4205}}} = 16.422m.$$

For *k*=4, the 16-PSK boundary, which is the inner ring,

$$R_{\max(16-PSK)} = 20 \times \sqrt[4]{\frac{10^{1.0778}}{10^{1.87}}} = 12.6774m.$$

Next, we use these $R_{\max}$ values to implement the region partition of our multi-modulation scheme. As a specific example, we again assume that 100 sensor nodes are distributed within the exciter's coverage area following a uniform distribution. Thus, the percentage of nodes with different modulations is proportional to the area of these three regions (as per eq. (10)). For the first region with 16-PSK modulation, the area is $A_{(16-PSK)} = \pi R^2_{\max(16-PSK)}$; for the second region with 8-PSK modulation, the area is $A_{(8-PSK)} = \pi R^2_{\max(8-PSK)} - \pi R^2_{\max(16-PSK)}$; for the last region with QPSK modulation, the area is $A_{(QPSK)} = \pi R^2_{\max(QPSK)} - \pi R^2_{\max(8-PSK)}$. The coverage area is $R_{cover} = 30.5m$, and $R_{\max(QPSK)} = 20m$, which is the furthest exciter-to-node distance. Thus, using the region partition equations that we obtained above, the 100 nodes are distributed in the range of $0 \sim 20m$ from the central point which represents the location of the exciter. By eq. (10), we have 33 nodes using QPSK, 27 nodes using 8-PSK, and 40 nodes using 16-PSK.

Next, we can compare the performance of the proposed multi-modulation scheme (with QPSK, 8-PSK, and 16-PSK in the different regions and with the distribution of sensor nodes following the region partition above) with the three cases of the single-modulation scheme of either QPSK, 8-PSK, or 16-PSK. We assume that at the

beginning of the first cycle, all the nodes have no energy stored. The charging time is then calculated by eq. (9). Assuming $t_{query} = 0.01sec$, the results of the comparison are shown in Table 3.

Table 3. Comparison of cycle times for the three modulation schemes

	Query	Charging time	Transmis-sion Time	Cycle Time
Multi modulation (QPSK, 8-PSK, 16-PSK)	0.01	1.2798	2.8436	4.1334
Single modulation (QPSK)	0.01	1.2798	4	5.2898
Single modulation (8-PSK)	0.01	2.7865	2.68	5.4765
Single modulation (16-PSK)	0.01	7.8445	2	9.8545

Based on the comparison in Table 3, in this example, the proposed multi-modulation scheme results in significantly shorter cycle time relative to all the three single-modulation schemes of either QPSK, 8-PSK, or 16-PSK. If we label the total transmission time in a cycle as t_{total}, the throughput improvement is calculated by eq. (13). Comparing with the most efficient single-modulation QPSK in Table 3, we gain about 28% in throughput improvement.

In evaluating the performance of the different schemes, we need to take into consideration the maximal distance of a sensor node to the exciter, which will change in different networks, which in the case of M-PSK is $R_{\max(QPSK)}$. In the Fig. 6, we show the total cycle time to maximal node-to-exciter distance diagram for multi-modulation and single-modulation schemes of M-PSK.

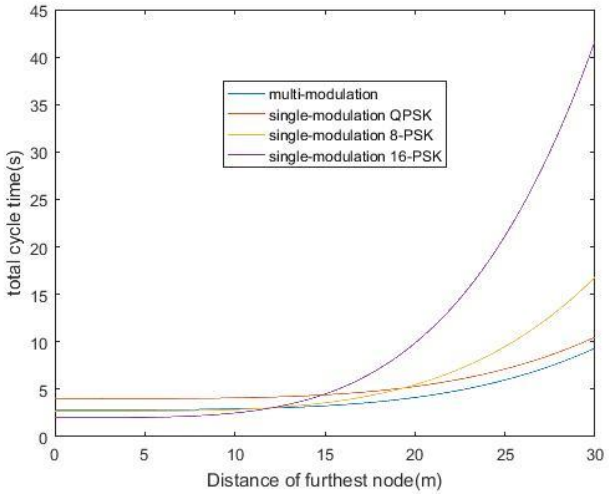

Fig. 6: Comparison of cycle times for different schemes

By eq. (9) and eq. (12), the improvement of the cycle time follows equation with only one variable R. As can be seen from Fig. 6, the "best" choice of the scheme depends on the maximal node-to-exciter distance. For instance, for small maximal node-to-exciter distances, the single modulation 16-PSK results in the shortest cycle, while for large maximal node-to-exciter distances, the multi-modulation scheme leads to the shortest cycle time.

To show a more comprehensive performance evaluation of our multi-modulation scheme, we also compare the following three multi-modulation schemes with the PSK multi-modulation scheme of a single-exciter network:

1. Multi-modulation scheme for a multi-exciter network applying M-PSK modulations: In multi-exciter networks, the charging time is calculated by (18), and the region partition follows Fig. 5.
2. Multi-modulation scheme for a single-exciter network applying M-QAM modulations: QAM multi-modulation scheme with M equal to 4, 8, 16.[5]
3. Multi-modulation scheme for a single-exciter network applying M-PAM modulations: PAM multi-modulation scheme with M equal to 2, 4, 8.[6]

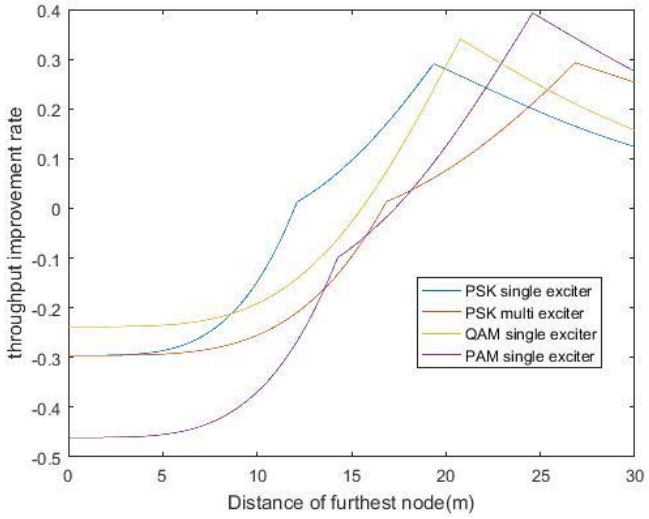

Fig. 7: Comparison of throughput improvement of the different multi-modulation schemes vs. the "best" single-modulation scheme

[5] The function of BER vs $\frac{E_b}{N_0}$ for the QAM and the PAM schemes are evaluated using the Matlab BER tool.

[6] For M-PSK scheme, BPSK and QPSK have the same $\frac{E_b}{N_0}$ at $BER = 10^{-6}$, so we cannot use BPSK, together with QPSK. For M-QAM scheme, 2-QAM cannot be found in the Matlab BER tool, so we use 4-QAM as the lowest order modulation.

Next, we evaluate the throughput of all these three multi-modulation schemes, together with the M-PSK scheme with a single-exciter. The throughput improvement is calculated by eq. (13), following the results in Fig. 6; for any maximal node-to-exciter distance, we should compare the throughput with the "best" (i.e., shortest cycle time) scheme. In Fig. 7, we show the comparison of the throughput improvement or degradation (based on eq. (13)) for the above three schemes, together with the previously discussed PSK single exciter case, relative to the performance of the multi-modulation schemes. With the exceptions outlined below, most of the parameters remain the same as in Table 3.[7]. As can be seen from Fig. 7, in our example, the multi-modulation scheme results in throughput improvement for networks with the maximal node-to-exciter distance greater than about 17 m. The improvement depends on the maximal node-to-exciter distance, but is most pronounced for larger networks. (The singular points in Fig. 7 are due to the fact that at these points the choice of the "best" scheme changes. For example, in Fig. 6, we observe that the choice of the "best" M-PSK scheme changes at a different maximal exciter-to-exciter distance; those "best" choices will now be used in eq. (13) for comparison with the multi-modulation scheme. In Fig. 7, the throughput of each curve is calculated at each maximal node-to-exciter distance for the "best" single-modulation scheme of the particular modulation family.)

In conclusion, the throughput improvement by our multi-modulation scheme is significant, as shown in Fig. 7 (e.g., up to nearly 40% improvement for the PAM scheme). However, the improvement depends on the maximal exciter-to-node distance, and for different schemes the throughput improvement curves are different. To maximize the benefits of the multi-modulation scheme, a network designer should choose the best multi-modulation scheme according to the furthest exciter-to-node distance and the throughput improvement curves in Fig. 7.

6 Conclusion and Future Work

In this paper, we propose a multi-modulation scheme to optimize the throughput of RFID Sensor Networks by minimizing the single cycle time of the network. Our scheme is applied to WSIP sensor nodes whose circuits harvest energy for communication and are able to implement different modulation methods. By applying different modulation methods in the nodes according to their distance to the exciter, our multi-modulation scheme minimizes the cycle time by saving the charging time of nodes located further from the exciter or by saving on the transmission time of nodes closer to the exciter, as compared with traditional single-modulation schemes. Our scheme could be applied to both the single-exciter network and multi-exciter network. We demonstrated an improvement of up to 40% of throughput according to our evaluation results. Our proposed scheme is in particular applicable to large scale / dense RFID Sensor Networks.

---

[7] Based on eq. (10), since the $\frac{E_b}{N_0}$ obtained from the Maltab BER tool for the QAM and the PAM schemes are different from PSK, the region partitions for QAM and PAM schemes are different from that of the PSK scheme. As a result, the number of nodes for different regions are changed as well. In addition, since we apply 2-PAM, 4-PAM, and 8-PAM in the PAM scheme, the transmission time for sensor nodes is changed to: 0.08sec, 0.04sec, and 0.0268sec, respectively

References

1. Sample, A., BUETTNER, M., & GREENSTEIN, B.:.Revisiting smart dust with RFID sensor networks. In: Proceedings of the 7th ACM Workshop on Hot Topics in Networks (HotNets-VII) (2008).
2. Buettner, M., Prasad, R., Sample, A., Yeager, D., Greenstein, B., Smith, J. R., & Wetherall, D.: RFID sensor networks with the Intel WISP. In: Proceedings of the 6th ACM conference on Embedded network sensor systems (2008).
3. Passive Radio Frequency Tags and Sensors for Process Monitoring in Advanced Reactors, https://www.energy.gov/sites/prod/files/2019/04/f61/Dirac%20FY2019-1%20Summary-Abstract%20ARD-19-1-16359.pdf, last accessed 10/28/2020.
4. Kalansuriya, P., Bhattacharyya, R., & Sarma, S.: A novel communication method for semi-passive RFID based sensors. In: 2014 IEEE International Conference on Communications (ICC). IEEE (2014).
5. Jia, X., Feng, Q., Fan, T., & Lei, Q.: RFID technology and its applications in Internet of Things (IoT). In: 2012 2nd international conference on consumer electronics, Communications and networks (CECNet), pp. 1282-1285. IEEE (2012).
6. Kim, T. H., Ramos, C., & Mohammed, S.: Smart city and IoT, pp. 159-162(2017).
7. Ahson, S. A., & Ilyas, M.: RFID handbook: applications, technology, security, and privacy. CRC press (2017).
8. Currie, I. A., & Marina, M. K.: Experimental evaluation of read performance for RFID-based mobile sensor data gathering applications. In: Proceedings of the 7th International Conference on Mobile and Ubiquitous Multimedia, pp. 92-95 (2008).
9. Alhassoun, M., Varner, M. A., & Durgin, G. D.: Design and evaluation of a multi-modulation retrodirective RFID tag. In: 2018 IEEE International Conference on RFID (RFID), pp. 1-8. IEEE (2018).
10. Wilas, J., Jirasereeamornkul, K., & Kumhom, P.: Power harvester design for semi-passive UHF RFID tag using a tunable impedance transformation. In: 2009 9th International symposium on communications and information technology, pp. 1441-1445. IEEE (2009).
11. Thomas, S. J., Wheeler, E., Teizer, J., & Reynolds, M. S.: Quadrature amplitude modulated backscatter in passive and semipassive UHF RFID systems. IEEE Transactions on Microwave Theory and Techniques, 60(4), 1175-1182 (2012).
12. Thomas, S. J., & Reynolds, M. S.: A 96 Mbit/sec, 15.5 pJ/bit 16-QAM modulator for UHF backscatter communication. In: 2012 IEEE International Conference on RFID (RFID), pp. 185-190. IEEE (2012).
13. d'Errico, R., Bottazzi, M., Natali, F., Savioli, E., Bartoletti, S., Conti, A., ... & Ouvry, L.: An UWB-UHF semi-passive RFID system for localization and tracking applications. In: 2012 IEEE International Conference on RFID-Technologies and Applications (RFID-TA), pp. 18-23. IEEE (2012).
14. Athalye, A., Savic, V., Bolic, M., & Djuric, P. M.: Novel semi-passive RFID system for indoor localization. IEEE Sensors Journal, 13(2), 528-537 (2012).
15. Zhen, B., Mizuno, K., Kobayashi, M., & Shimizu, M.: Pulse position modulation for active RFID system. In: 11th International Conference on Parallel and Distributed Systems (ICPADS'05), vol. 2, pp. 58-62. IEEE (2005).
16. Decarli, N., Guidi, F., Conti, A., & Dardari, D.: Interference and clock drift effects in UWB RFID systems using backscatter modulation. In: 2012 IEEE International Conference on Ultra-Wideband, pp. 546-550. IEEE (2012).
17. Ramos, A., Lazaro, A., & Girbau, D.: Semi-passive time-domain UWB RFID system. IEEE transactions on microwave theory and techniques, 61(4), 1700-1708 (2013).

18. Hannan, M. A., Islam, M., Samad, S. A., & Hussain, A.: RFID communication using software defined radio technique. In: AIP Conference Proceedings, Vol. 1247, No. 1, pp. 41-55. American Institute of Physics (2010).
19. Proloy, M., Hoq, R., & Ahmed, S. M.: Comparative analysis of various wireless digital modulation techniques with different channel coding schemes under AWGN channel. Doctoral dissertation, East West University (2016).
20. Meghdadi, V.: BER calculation. Wireless Communications (2008).
21. Lee, M. H., Yao, C. Y., & Liu, H. C.: Passive tag for multi-carrier RFID systems. In: 2011 IEEE 17th International Conference on Parallel and Distributed Systems, pp. 872-876. IEEE (2011).
22. Wireless network lesson on modulation methods, https://www.usna.edu/ECE/ec312/Lessons/wireless/EC312_Lesson_24_Sup.pdf, last accessed 2019/10/31.
23. How RFID works on howstuffworks, https://electronics.howstuffworks.com/gadgets/high-tech-gadgets/rfid.htm#pt3, last accessed 2020/08/13.
24. Modulation, Power and bandwidth introduction, https://www.aticourses.com/sampler/Modulation_Power_Bandwidth.pdf, last accessed 202008/13.
25. Zhou, Z., Gupta, H., Das, S. R., & Zhu, X.: Slotted scheduled tag access in multi-reader RFID systems. In: 2007 IEEE International Conference on Network Protocols, pp. 61-70. IEEE (2007).
26. Seetharam, D., & Fletcher, R.: Battery-powered RFID. In: 1st ACM Workshop on Convergence of RFID and Wireless Sensor Networks and their Applications (2007).
27. Understanding passive RFID technology, https://rfidworld.ca/understanding-passive-rfid-radio-frequency-identification-technology/1294, last accessed 2020/08/13.
28. Zhang, Y., Li, X., & Amin, M.: Principles and techniques of RFID positioning. In: Rfid Systems, pp.389(2010).
29. RFID antenna gain and range, https://www.eetimes.com/document.asp?doc_id=1276310, last accessed 2020/08/13.
30. Pursula, P., Kiviranta, M., & Seppa, H.: UHF RFID reader with reflected power canceller. IEEE Microwave and Wireless Components Letters, 19(1), 48-50 (2008).
31. Thomas, S., & Reynolds, M. S.: QAM backscatter for passive UHF RFID tags. In: 2010 IEEE International Conference on RFID (IEEE RFID 2010), pp. 210-214. IEEE (2010).
32. Rembold, B.: Optimum modulation efficiency and sideband backscatter power response of RFID-tags. Frequenz, 63(1), 9 (2009).